

Implementing the Hybrid Segmentation with Adaptive Densenet and Improved Heuristic Approach for Classifying the Prostate Cancer

Thirupathanna Kurva¹, Mudigonda Malini², Medi Sriinivas³, K. E. Ch.Vidyasagar⁴

Submitted: 14/05/2024 Revised: 24/06/2024 Accepted: 04/07/2024

Abstract: Early detection of prostate cancer is challenging due to its subtle symptoms, which has led to the exploration of deep learning algorithms to improve diagnostic accuracy of MRI images. In response to these challenges, the development of a computer-aided detection (CAD) system with segmentation and categorization techniques has become increasingly important. In this research, a novel hybrid prostate cancer detection method that utilizes segmentation and adaptive model classification is proposed to overcome the current limitations. The proposed method includes three main phases: Image acquisition, segmentation and classification. At the beginning, images are extracted from publicly available online databases. Then, these images are subjected to Dilated Hybrid Segmentation (DHS), which integrates TransUnet with Segnet to accurately delineate prostate lesions. Finally, the segmented images are fed into the Adaptive and Attentive Multiscale Densenet (AAMDNet) classification model, where certain hyper parameters are optimized using the Enhanced Capuchin Search Algorithm (ECapSA). The performance of the model is then evaluated using various metrics. Compared to conventional approaches, this novel system delivers impressive results, and shows higher accuracy in the classification of prostate cancer.

Keywords: Prostate Cancer Classification; Prostate Image; TransUnet and Segnet; Dilated Hybrid Segmentation; Adaptive and Attentive Multiscale Densenet; Enhanced Capuchin Search Algorithm.

1. Introduction

The prostate, a vital part of the male reproductive system, is small, about the size of a walnut, and lies below the urinary tract. Prostate cancer, a common type of cancer in men, originates in this gland [1]. The abnormal proliferation of cells in the prostate tissue leads to the formation of tumors, which can be benign or malignant [2]. Malignant tumors can metastasize and spread to the surrounding tissue. Prostate cancer mainly affects older people, but can also manifest itself without any recognizable symptoms and often progresses slowly [3]. In certain cases, it can progress aggressively and require therapeutic intervention [4].

Digital rectal examinations (DRE), blood tests for prostate-specific antigen (PSA) and biopsies of the prostate tissue are usually to detect prostate cancer. These diagnostic methods help to determine the presence and severity of prostate cancer [5]. Treatment options for prostate cancer depend on the stage and aggressiveness of the cancer. Early detection and appropriate treatment significantly improve the prognosis. Regular screening and discussions with the doctor are crucial, especially for men over the age of 50 or for men with a family history of the disease [6]. The classification of

prostate cancer assesses factors such as stage, grade and risk [7]. This classification is essential for determining appropriate treatment strategies and predicting disease progression [8].

The classification of prostate cancer is very complex and represents a major challenge for the treatment of the disease [9]. Accurate classification is crucial as it serves as a basis for treatment decisions and prognostic assessments [10]. However, several factors contribute to the difficulties associated with this process [11]. Prostate cancer is inherently heterogeneous, exhibiting different characteristics from patient to patient and even within individual tumors. This variability makes accurate classification and prediction of disease behavior difficult.

In the field of medical image analysis, particularly in the categorization and detection of prostate cancer, machine learning algorithms have proven to be powerful tools [12]. These algorithms, which use multi-layer synthetic neural networks, are characterized by the extraction of complex features and patterns from medical image data. In particular, deep learning techniques have shown promise in improving the accuracy, efficacy, and ability to handle complexity in prostate cancer categorization [13]. By using artificial neural networks to decipher complex medical image data, deep learning algorithms have revolutionized the categorization and diagnosis of prostate cancer [14]. These innovative techniques have the potential to increase the accuracy, efficiency and impartiality of prostate cancer assessment, improving patient outcomes and expanding our understanding of the disease. They therefore represent a significant advance in the field of medical image analysis and offer new opportunities for more accurate and effective diagnosis and treatment of prostate cancer [15].

The primary objectives of the developed model can be elucidated as follows.

1 Research Scholar Department of Biomedical Engineering, University College of Engineering Osmania University, Hyderabad, India. thirukurva@gmail.com

2 Professor, Department of Biomedical Engineering, University College of Engineering Osmania University, Hyderabad, India. malini.m@uceou.edu

3 Professor, Department of Biomedical Engineering, University College of Engineering Osmania University, Hyderabad, India. medisrinivas@osmania.ac.in

4 Professor, Department of Biomedical Engineering, University College of Engineering Osmania University, Hyderabad, India. vidyasagar.ou@gmail.com

1. Using TransUnet and SegNet to accurately segment prostate cancer regions in medical images, utilizing their strengths in dealing with complex anatomical structures.
2. Implementing an Adaptive Attentive Multiscale DenseNet to classify segmented regions to ensure high accuracy in identifying different stages and types of prostate cancer.
3. Applying the advanced Capuchin search algorithm for hyper parameter optimization to fine-tune the segmentation and classification models to maximize their performance and efficiency.
4. Ensuring that Adaptive Attentive Multiscale DenseNet effectively captures multiscale features from segmented regions, increasing the accuracy of prostate cancer classification.
5. Testing and validating the segmentation and classification models against established prostate cancer imaging datasets and compare their performance with existing state-of-the-art methods.
6. Contributing to the medical imaging and prostate cancer research by providing a novel and effective approach to cancer segmentation, classification and optimization.

2. Existing Works

2.1. Related Works

Classification of prostate cancer is crucial aspect of treating the disease, as it involves grading and characterizing the cancer based on key factors such as stage, grade and risk level. Accurate classification plays a crucial role in determining the most appropriate treatment strategies and predicting the patient outcomes. Various methods and systems are for this purpose, each with their own strengths and challenges. A detailed overview of the different methods is shown in Table I and is discussed in the following paragraphs.

Table I: Features and Challenges of Existing Deep Learning Based Prostate Cancer Classification System

Author [citation]	Metho-dology	Features	Challenges
Shrestha <i>et al.</i> [16]	DNN	It can model complex, non-linear relationships in data. It can automatically learn hierarchical representations from data.	Hyper parameter tuning can be challenging.
Garg <i>et al.</i> [17]	CAD	Reduces the time and effort required for design and engineering tasks. Allows for accurate simulations and testing before physical production.	Complex designs can be computationally intensive to render and analyze.
Chahal <i>et al.</i> [18]	Unet	Specifically designed for image segmentation tasks, especially in medical imaging.	It may require a large amount of labeled data for training.
Guiqin <i>et al.</i> [19]	CNN	It automatically learns hierarchical features from data.	It requires substantial computational resources for training deep networks
Pääkkönen <i>et al.</i> [20]	ML	It can make predictions and decisions based on data.	It requires feature engineering in many cases.
Pushpak <i>et al.</i> [21]	DL	It can automatically extract features from raw data.	Training can be time-consuming and computationally expensive.
Yuchun <i>et al.</i> [22]	DL	It can model complex, non-linear relationships in data. It can automatically learn hierarchical representations from data.	Tuning the hyperparameters can be challenge.

2.2. Research Gaps and Challenges

Deep Neural Networks (DNNs) were developed to model complex, non-linear relationships in data. They automatically learn hierarchical representations, which can be of great use in capturing complex patterns in medical images and other types of data relevant to prostate cancer classification. DNNs consist of multiple layers of interconnected neurons that enable them to learn from large amounts of data. However, the challenge lies in tuning the numerous parameters within these networks. This tuning process is crucial for achieving high accuracy, but is also one of the most difficult aspects of working with DNNs, as it requires significant computational resources and expertise.

Computer-aided design (CAD) systems are used to streamline design and development engineering tasks. In the context of prostate cancer, CAD can be used to create detailed models and simulations of the prostate and surrounding tissue. These simulations allow accurate testing and prediction of treatment outcomes prior to surgery. However, the intricate designs created by CAD systems can be very computationally intensive to

visualize and analyze, posing a challenge in terms of the computing power and time required.

Unet is a specialized deep learning architecture tailored to image segmentation tasks, especially in medical imaging. It is extremely effective in delineating structures in medical images, such as tumors in prostate scans. The Unet architecture consists of a contracting path to capture the context and a symmetric expanding path that enables precise localization. Despite its remarkable capabilities, Unet often requires a large amount of labeled training data to work effectively, which can be a limitation in medical fields where labeled data is scarce.

Convolutional Neural Networks (CNNs) are particularly suitable for processing and analyzing visual data. They are able to automatically learn hierarchical features from raw input images, making them ideal for tasks such as detecting and classifying cancer regions in prostate images. CNNs use convolutional layers to extract features and pooling layers to reduce dimensionality, followed by fully connected layers for classification. However, training deep CNNs can be resource intensive and requires a lot of computational power and time.

Deep learning (DL) encompasses a range of architectures, including DNNs, CNNs and others, that are capable of automatically extracting features from raw data. This ability to learn directly from the data without the need for manual feature processing is particularly beneficial for complex classification tasks such as prostate cancer. Despite its promising capabilities, deep learning requires extensive computational resources and time for training and hyper parameter tuning remains a major challenge. Machine learning (ML) Traditional machine learning methods facilitate prediction and decision making based on data. These methods often require manual feature engineering, where experts must identify and extract relevant features from the raw data before feeding them into the ML algorithms. While ML methods can be very effective, manual feature engineering can be time-consuming and requires extensive expertise.

In summary, each of these methods offers distinct advantages for prostate cancer classification, from the high-dimensional capabilities of SVM to the powerful feature learning of deep neural networks and CNNs. However, they also bring specific challenges, such as the need for computational resources, experience in tuning hyper parameters and the availability of labeled training data. The Accurate and efficient classification of prostate cancer depends on the correct application of these methods to ensure optimal treatment strategies and a better prognosis for patients.

3. Explanation of the Proposed Classification Model for Prostate Cancer: Improved Heuristic Algorithm

3.1. Collection of raw images

In the initial phase, images relevant to prostate cancer are collected for later processing by a categorization model.

Dataset-1: "Access Date: 2023-09-26". This dataset is primarily about prostate cancer, with a focus on the "Prostate central gland and peripheral zone." The dataset comprises a total of 394 images, of which 75% are allocated for training purposes, while the remaining 25% are designated for testing.

All studies [23] included T2-weighted (T2W), proton density-weighted (PD-W), dynamic contrast enhanced (DCE), and diffusion-weighted (DW) imaging. Images were acquired with two different types of Siemens 3T MR scanners, the MAGNETOM Trio and Skyra. The T2-weighted images were acquired with a turbo spin echo sequence and had a resolution of around 0.5 mm in plane and a slice thickness of 3.6 mm. The DCE time series was acquired using a 3-D turbo flash gradient echo sequence with a resolution of approximately 1.5 mm, a slice thickness of 4 mm and a temporal resolution of 3.5 s. The proton density weighted image was acquired before to the DCE time series using the same sequence with different echo and repetition times and a different flip angle. Finally, the DWI series were acquired with a single-shot echo planar imaging sequence with a resolution of 2 mm in-plane and 3.6 mm slice thickness and with diffusion-encoding gradients in three directions. Three b-values were acquired (50, 400, and 800), and subsequently, the ADC map was calculated by the scanner software. All images were acquired without an endorectal coil.

Dataset-2: "Access Date: 2023-09-25". It includes [23] data comprises a total of 1083 images. For the purposes of model development, 75% of these images are allocated for training, with the remaining 25% reserved for testing.

Prostate cancer T1- and T2-weighted magnetic resonance images (MRIs) were acquired on a 1.5 T Philips Achieva by combined surface and endorectal coil, including dynamic contrast-enhanced images obtained prior to, during and after I.V. administration of 0.1 mmol/kg body weight of Gadolinium-DTPA (pentetic acid).

3.2. Adaptive Concept in Prostate Cancer Classification Model

Prostate cancer can progress, with low-grade cancers initially becoming more aggressive. Regular monitoring is essential to track these changes and adjust treatment as needed. The proposed ECapSA-based classification model, shown in Figure 1, is designed to improve diagnostic accuracy and treatment efficacy.

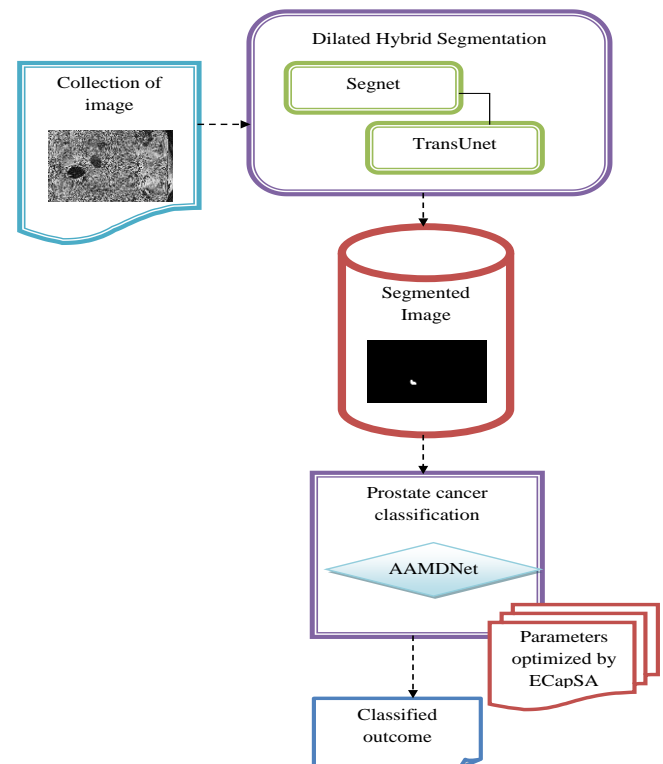


Fig. 1. Framework of developed ECapSA based prostate cancer classification model

The aim of this work is to develop an advanced classification model for prostate cancer by integrating heuristic and deep learning methods to improve diagnostic accuracy. Input images are collected from publicly available sources to create a diverse dataset. TransUnet and SegNet are then used for accurate segmentation of prostate regions, which is essential for improving classification accuracy.

The segmented images are classified as cancerous or non-cancerous using the AAMDNet model, which utilizes deep learning for high accuracy. The performance of the model is evaluated using metrics such as sensitivity, specificity, F1 score and accuracy to ensure its reliability and precision in classifying prostate cancer.

3.3. Identification of Abnormalities using Dilated Hybrid Segmentation Model

3.3.1. TransUnet

The ability of the U-net to accurately separate objects or regions of interest in photographs can be enhanced by the transformer's ability to view the entire image. A TransUnet approach [24] combines the advantages of the transformer and U-net designs and can use Transformer-based mechanisms of self-attention to

recognize complex relationships between individual pixels in an image, or voxels in the case of 3D image

The output of the k_{th} layer of a transformer encoder consists of K layers of Multihead Self-Attention (MSA) and Multi-Layer Perceptron (MLP) blocks. Let's denote the input to the k_{th} layer as k^l , where l is the layer index $l=1,2,...,L$. The output of the l_{th} layer can be written as following Eq.(1) and Eq.(2).

$$H_l^s = MSA(KM(H_l^s - 1) + H_l^s - 1) \quad (1)$$

$$H_l^s = MLP(KM(H_l^s) + H_l^s) \quad (2)$$

One simple segmentation technique is to simply raise the encoded

representation of characteristics $S_l \in k^{\frac{IO}{P^2} \times j}$ to full fidelity in order to anticipate the dense result. The scope of the coded

component must first be modified from $\frac{IO}{P^2}$ to $\frac{I}{P} \times \frac{K}{P}$ in order to restore spatial harmony. The feature map is immediately bilinear up sampled to the greatest quality in order to condense the channel length of the 1x1 reconfiguration characteristic to the entire number of classes, anticipating the final segmentation outcome. This naive extending baseline is labeled $m \times m$ in the decoding scheme for the ensuing studies.

The combination of converters with naive development leads to acceptable efficiency, but often low-level information is lost, resulting in lower quality image restoration. TransUnet solves this problem by using a CNN transformer encoder and a broadcast up-sampler for accurate localization.

CNN-Transformer: TransUnet uses a CNN-transformer hybrid technique instead of using only transformers as encoded data, where CNN is first used as a feature extractor to create a map of features for the input data. Instead of raw images, the patch anchor is applied to patches created from the CNN mapping of features. Our combined CNN-transformer-encoder is better than a transformer alone. We chose this design because it allows us to use high-quality CNN feature maps in the decoder in the meantime.

Cascaded up sampler: Offer a cascaded upsampler (CUP) that consists of a number of expanding procedures, to decode the

hidden feature $S_l \in k^{\frac{IO}{P^2} \times j}$ and generate $\frac{I}{P} \times \frac{K}{P} \times D$ the segmented mask in the end. After modifying the hidden feature

sequence to take the form of $\frac{I}{P} \times \frac{K}{P} \times Y \times w$, we produce CUP by falling several expanding blocks to achieve the whole solution from, where every component comprises a sequentially a ReLU layer, 33 expanding operator and 33 convolutions layer. Using skip-connections, Cups and the whole encoder's u-shaped architecture enables feature aggregate at various fidelity levels. Fig. 2 shows the architecture diagram for TransUnet.

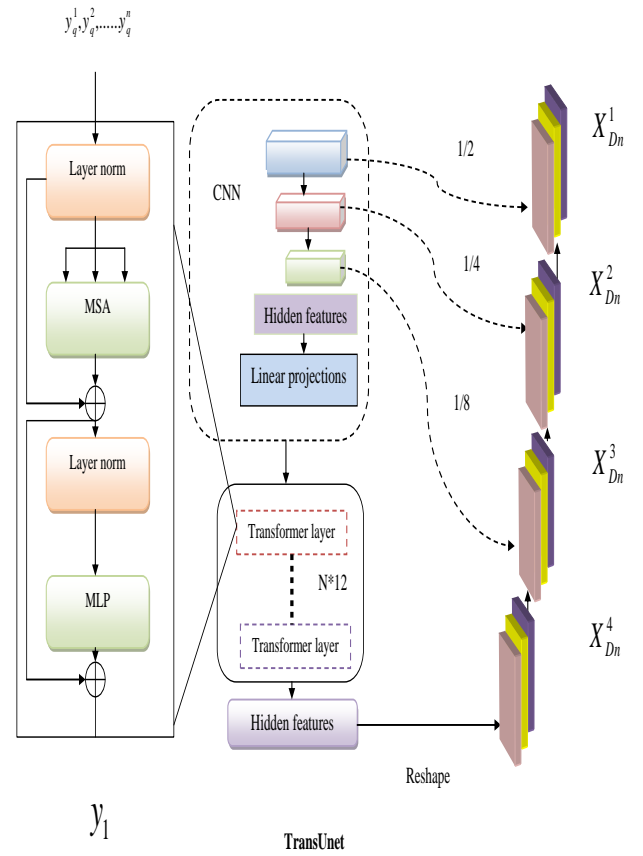


Fig. 2. Architecture diagram for TransUnet

3.3.2. Segnet

An encoding network and an associated decoding system, followed by a final pixel-wise categorization layer, form the two main components of SegNet [25]. The VGG16 system, which was originally developed for object recognition tasks, started with 13 convolutional layers, and the coding network also consists of a total of 13 convolutional layers. This design allows us to use pre-trained weights from VGG16 as a starting point for training SegNet. These weights have been optimized for categorization in large datasets.

SegNet uses a tactic that omits the fully concatenated layers typically present in categorization systems, which has benefits beyond determining weights. Instead, it places a greater priority on maintaining high-resolution feature maps in the output of the lowest level encoder. Compared to other modern architectures, this not only preserves the geographic data, but also drastically reduces the number of parameters in the SegNet decoder network. The decoder consists of a total of 13 layers, as each layer in the network that makes up the encoder has a corresponding layer in the decoder network. The final output of the decoder is then provided with a multi-class softmax classifier. This classifier provides pixel-accurate segment results, which are essential for applications such as semantic segmentation. It does this by assigning an individual class probability to each pixel.

In SegNet, each coding layer uses a filter bank to create feature maps, which are standardized by batch normalization and enhanced with ReLU. The output is down sampled by a factor of 2 using 2x2 Max Pooling to ensure translation invariance and insensitivity to spatial variations. However, this under sampling reduces the dimensions of the feature maps.

For applications with limited memory, it is impractical to store all features after down sampling. Instead, only the indices of the highest values in each 2x2 pooling window are stored, requiring only 2 bits per window. This method is more memory efficient than storing entire feature maps in float precision.

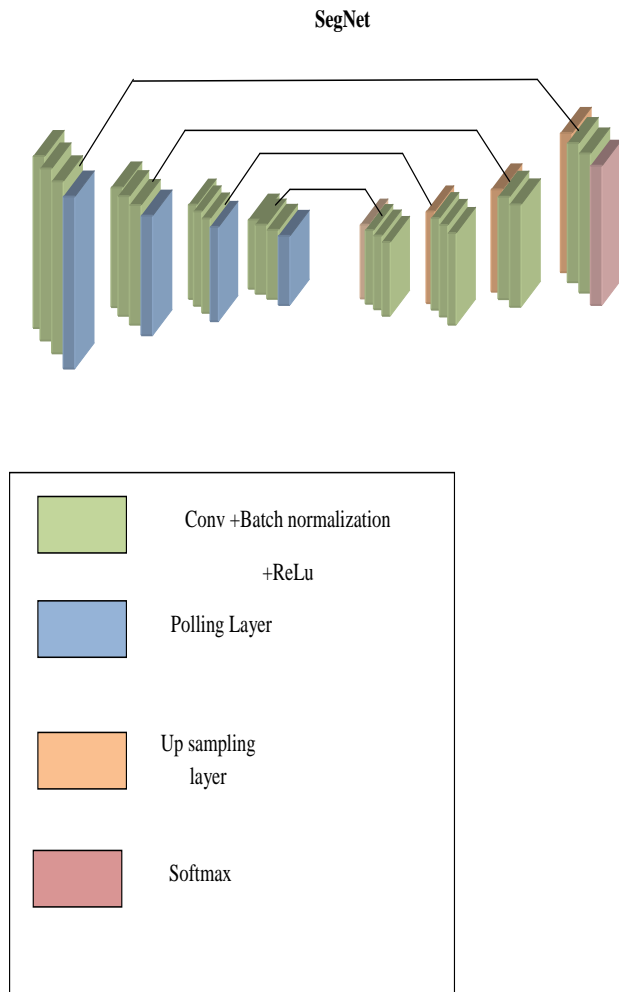


Fig. 3. Architecture diagram for SegNet

3.3.3. Dilated Hybrid Segmentation

Dilated SegNet and Dilated TransUnet are neural network variants for image segmentation that use dilated convolutions to capture information at multiple levels. DHS, hybrid architecture, combines these models for improved segmentation accuracy. The encoder, a dilated SegNet, extracts features from the input images, while the decoder, a dilated TransUnet, creates the final segmentation map. This approach leverages SegNet feature extraction and TransUnet modeling to improve segmentation tasks. The final result of our

DHS model is a segmented image TS_r^{seg} . Fig.4 shows the diagrammatic representation of the DHS for prostate cancer segmentation.

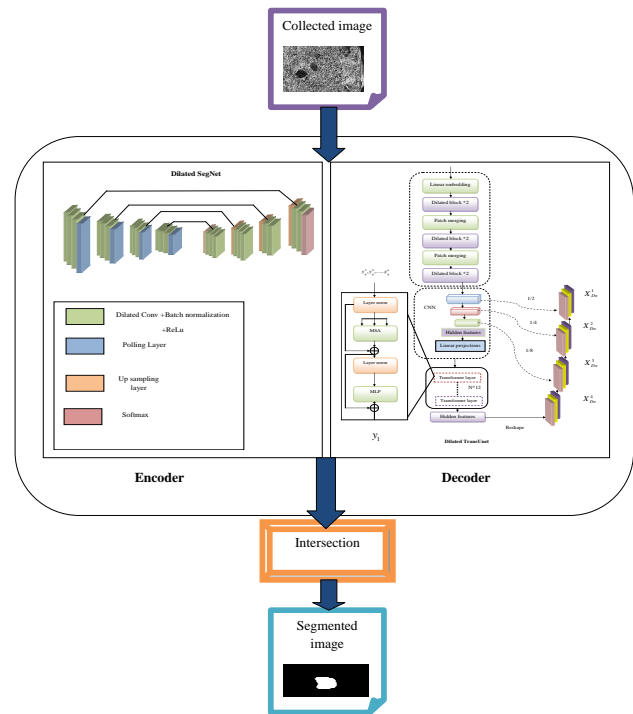


Fig. 4. Diagrammatic representation of the DHS for prostate cancer segmentation

Justification for Using Dilated SegNet, Dilated TransUnet, and DHS Over Other Segmentation Methods in the following paragraphs

3.3.4. Dilated SegNet

Dilated SegNet introduces dilated convolutions to increase the receptive field without additional downsampling. This captures a broader context while preserving fine details. Standard SegNet is based on pooling, which can lead to loss of information. U-Net captures information at multiple levels through a symmetric encoder-decoder structure, but relies on pooling and upsampling, which can lead to information loss. Dilated SegNet avoids this by using dilated convolutions directly.

3.3.5. Dilated TransUnet

CNN-based models, such as SegNet and U-Net, are characterized by local features but have problems with global context. Dilated TransUnet incorporates transformers to capture both local and global context to improve segmentation performance, especially for complex scenes. Pure Transformer models can struggle with fine-grained details. Dilated TransUnet mitigates this problem by integrating CNNs and dilated convolutions that ensure detailed local feature extraction. By adding Dilated Convolutions, Dilated TransUnet can capture features at multiple scales, improving the ability to segment objects of different sizes.

3.3.6. Dilated Hybrid Segmentation

The hybrid DHS architecture leverages the strengths of Dilated SegNet and Dilated TransUnet captures detailed local features and a comprehensive global context. Single model architectures may be deficient in one aspect or another. Specialized models are often tailored to specific tasks, such as medical imaging or street segmentation. DHS combines methods, making it adaptive and robust for different segmentation tasks. Simple ensemble methods combine predictions from multiple models. DHS deeply integrates the architectures, and enables better feature fusion and interaction, leading to more coherent and accurate segmentation results.

3.4. Prostate cancer classification using Adaptive and attentive based Deep Learning Network

3.4.1. Multiscale Densenet

Multi-Scale DenseNet retains the dense connectivity of the original DenseNet architecture. In DenseNet, each layer is directly connected to every other layer in a feed-forward manner. This dense connectivity supports gradient flow, feature reuse, and allows the network to learn rich representations. The multiscale DenseNet is explained in more detail below.

3.4.2. Multiscale Densenet:

To improve prostate classification, a multilevel approach is used iteratively at different scales to improve feature extraction. This results in a richer, more comprehensive and complementary feature set and improves the adaptability of the model and the ability to identify relevant features across multiple spatial or temporal scales.

3.4.3. DenseNet:

DenseNet [26] aims to improve the connectivity of neural networks by creating dense connections between layers. In contrast to conventional CNNs, where information is transferred incrementally, DenseNet allows each layer within a block to receive input from all previous layers. This dense data flow improves feature reuse, training gradient flow and storage efficiency.

Imagine that a network of convolutions made of layers propagates

a single picture, denoted as t_o , through the network's layers. Each layer referred to here as m and the layer—involves a non-linear change symbolized by $SL(\cdot)$. Batch Normalization (BN), Rectified Linear Unit (ReLU) and Convolution, pooling application are some of the procedures covered by this function. As shown in an undefined Eq. (13) popular feed forward network structures like AlexNet and VGG Net create links that link the k_{th} layer's outputs $(k-1)_{th}$ and inputs.

$$p_1 = SL(k-1) \quad (3)$$

Skip-connections are a novel addition to ResNet's design. These connections use the identity equation to include the layer's results $(k-1)_{th}$, represented as $(k-1)$, into the calculation process of the present layer. The subsequent Eq. (4) represents this technique.

$$p_1 = SL(k-1) + k-1 \quad (4)$$

The skip link design initially developed by ResNet is significantly improved by the thick connection strategy that DenseNet uses. With this method, the feature maps from the layer and all levels before it are concatenated into a structure called a dense block. As a result, the map features of the earlier layers are combined to

create the input for the final layer p_o, p_1, \dots, p_{m-1} . Eq. (5) beautifully illustrates this procedure.

$$p_1 = DF[p_o, p_1, \dots, p_{m-1}] \quad (5)$$

DenseNet offers a crucial tactic to solve the problem of decreasing signal strength due to increasing layer thickness and to improve overall performance. The design reduces signal attenuation by combining feature maps from different layers within a dense block. However, as the depth of net work increases, a problem arises. The number of channels in the overall feature map increases sharply,

which significantly increases the size of the network. DenseNet solves this problem by inserting a bottleneck layer between each layer in the dense block. The methods that make up this bottleneck layer are Rectified Linear Unit (ReLU), Batch Normalization (BN), 1x1 convolutional filters (conv), 2 BN, ReLU, and 3x 3 convolutions. Fig 5 shows the architecture diagram for Multiscale DenseNet.

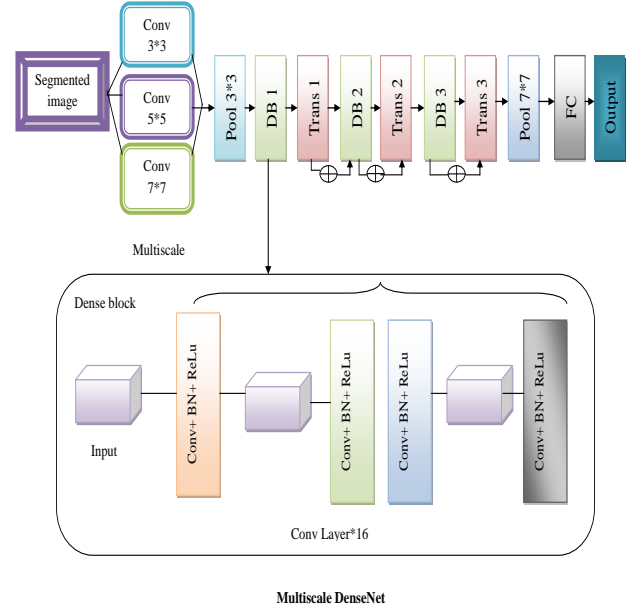


Fig. 5. Architecture diagram for Multiscale Densenet

3.4.4. Attention Mechanism

Machine learning and deep learning approaches often rely on the attention mechanism [26], especially for tasks such as automatic translation and text summarization. This mechanism helps the models to focus on specific data elements when generating results. The attention mechanism consists of three parts: Query, Key and Value.

The query represents what the model is interested in at a given time, derived from its hidden state, and is used to compute attention values. The key is compared to the query to determine which parts of the input data are relevant. The value associated with the attention values represents the information to focus on in the output, using the attention values as a guide (Equation 6).

$$Attention(l, m, n) = \text{softmax} \left(\frac{lm^t}{\sqrt{e_v}} \right) \quad (6)$$

The variable l, m and n is the query, key, and value matrixes. The attention mechanism works by calculating attention scores, often using some similarity metric between the query and key.

3.4.5. D.AAMDNet for Classification

The choice of the AAMDNet classifier for the prostate cancer classification system can be justified in the following paragraphs.

3.4.5.1. Advanced architecture

AAMDNet, a state-of-the-art deep learning model, provides a sophisticated architecture that excels in feature extraction and pattern recognition, which is critical for distinguishing between cancerous and non-cancerous regions in medical imaging.

3.4.5.2. Improved performance

Empirical results show significant performance improvements over other models. AAMDNet achieves 57% higher accuracy than Unet, 55% than Resunet, 67% than TransUnet and 48% than SegNet. This underlines its superior ability to accurately classify prostate cancer.

3.4.5.3. Efficient processing of complex data

AAMDNet is designed to process complex and high-dimensional data effectively. Images of prostate cancer often show subtle differences between cancerous and non-cancerous tissue, requiring a robust model that can capture these nuances.

3.4.5.4. Robust training mechanism

The architecture of AAMDNet enables efficient training and better convergence. This robustness ensures that the model can generalize well from the training data to unseen data, which is critical in medical applications where data variety and representation are critical.

3.4.5.5. Integration with segmentation models

AAMDNet can effectively utilize segmented images generated by advanced segmentation models such as TransUnet and SegNet. This integration ensures that the classifier works with well-defined regions of interest, increasing the accuracy of the classification process.

3.4.5.6. Scalability and adaptability

AAMDNet is scalable and adapted to different data sets and different sizes of input screens. This flexibility is important to accommodate the diversity of medical imaging data and to ensure that the model remains effective in different clinical environments.

3.4.5.7. Improvement over traditional models

Traditional models often unable to handle the intricacies of medical image classification due to their simpler architecture. AAMDNet's advanced design overcomes these limitations and provides a more refined and accurate approach to prostate cancer classification.

By choosing AAMDNet, the prostate cancer classification system utilises a state-of-the-art model that not only outperforms existing methods, but also provides a reliable and efficient solution for real-world medical applications.

The process begins with the input of a segmented image TS_r^{seg} , which is then forwarded to a multiscale analysis module. The multiscale module processes the image and generates a multiscale representation that is used by an attention mechanism. This enhanced representation is then fed into a DenseNet model for classification. The performance of DenseNet is influenced by the number of hidden neurons, the epochs and the steps per epoch. The optimization of these parameters is crucial for the balance between model complexity and generalization. Fine-tuning these parameters improves the accuracy, precision and MCC of the model and maximizes the predictive power and overall effectiveness. The objective function of the proposed system is described in Eq. (7).

$$AA_{obj} = \arg \max_{\{NE_{AA}^{den}, SP_{AA}^{den}, HN_{AA}^{den}\}} [Ac + Pr + MC] \quad (7)$$

Here the term $NE_{AA}^{den}, SP_{AA}^{den}$ and HN_{AA}^{den} defines the hidden neuron count, no of epochs and steps per epoch in DenseNet and the range is [5 - 255], [5 - 50] and [100 - 500]. Also the term Ac, Pr and Mc defines the accuracy, precision and MCC.

The mathematical formulation of Ac, Pr and Mc is described in Eq. (8), Eq.(9) and Eq.(10).

$$Ac = \frac{LK + PM}{LK + PM + LS + IU} \quad (8)$$

$$Pr = \frac{LK}{LK + PM} \quad (9)$$

$$MC = \frac{IU \times PM - PN \times PM}{\sqrt{(IU + LK)(IU + PM)(LK + PS)(TJ + IU)}} \quad (10)$$

"The variable LK ' represents instances of 'false negatives,' while the parameter PM denotes occurrences of 'false positive values.' The metrics LS and IU define 'true negatives' and 'true positives,' respectively. Fig. 6 shows the diagrammatic representation of the suggested AAMDNet for classification.

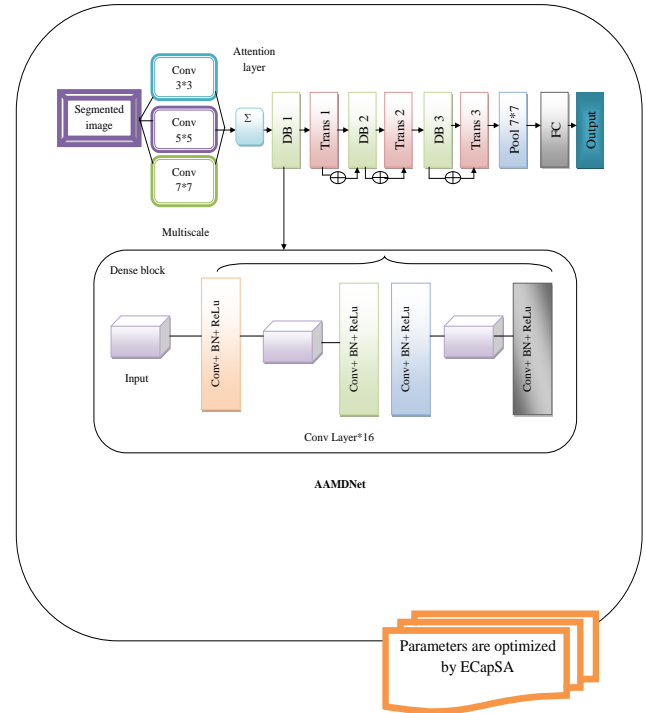


Fig. 6. Diagrammatic representation of the recommended AAMDNet for classification

3.5. Enhanced Capuchin Search Algorithm

The ECapSA approach introduces a novel strategy that prioritizes the maximization of variables to increase the reliability of optimization tasks, using the CapSA [27] algorithm as a standard. Effective search algorithms must be efficient in both time and space and quickly find optimal or near-optimal solutions. However, the high computational complexity can make some algorithms impractical for real-time or resource-constrained applications. Performance can also depend on the choice of parameters, making configuration difficult. To address these challenges, the recommended method uses Eq. (11) to calculate random values that help determine new positions.

$$\delta = \frac{(B_f)^2}{(W_f)^2} \quad (11)$$

In the equation presented above, the variables "best fitness value" and "worst fitness value" are denoted as B_f and W_f respectively, while the term δ signifies a randomly generated

position. The mathematical expression for ECapSA is depicted below.

In the CapSA algorithm, the capuchin monkey population is divided into two groups: the alpha group (leaders and accompanying capuchins) and the followers. The leaders find food sources and guide the followers, who update their position by following the leaders or other followers. Inspired by the intelligent foraging behavior of capuchin monkeys, CapSA offers parallels between their problem-solving abilities and the optimization of search algorithms in computer science and engineering.

The formula for calculating the velocity of the a_{th} capuchin in the b_{th} dimension within the CapSA algorithm is represented as described in Eq.(12).

$$C_a^b = E\beta_a^b + r_1(k_{best}^a - k_b^a)\delta_1 + r_2(U_b - k_b^a)\delta_2 \quad (12)$$

Here, C_a^b is the a_{th} capuchin's current velocity in the b_{th} dimensions, k_b^a is the a_{th} alpha capuchin's current place in the b_{th} dimensions, k_{best}^a is the place with the ideal fitness discovered thus quite for the a_{th} capuchin in the b_{th} dimensions, r_1 and r_2 are two speed variables that regulate the impacts. The term δ defines the random number, in conventional approaches the random number ranges from 0, 1 and this leads to many optimal and convergence problems.

In order to mitigate these errors, employ the proposed formulation outlined in Equation (1). The formula for updating the current velocity of the a_{th} capuchin in the b_{th} dimension based on its previous velocity, as described in Eq. (13), can be expressed as follows:

$$\rho = \omega_m - (\omega_s - \omega_l) \times (k / s)^2 \quad (13)$$

The position of alpha capuchins in the CapSA algorithm, the term k_b^a is defined in line with the definition given in Eq. (14), more especially as they take part in doing so.

$$k_b^a = U_b + \frac{T_{ab}(c_a^b)^2 \sin(2\theta)}{s} \quad (14)$$

Here, T_{ab} stands for the likelihood that the capuchins' tail will give balance, s stands for the strength of the force of gravity, this, according to Eq. (15), equals 9.81 and represents the point at which the capuchins will jump.

$$\theta = \frac{3}{2} \delta \quad (15)$$

Alpha capuchins in the CapSA are characterized as being at the location given by Eq. (16) as they use a jumping technique to forage for nourishment on the banks of rivers:

$$k_b^a = U_b + \frac{T_{ab}(c_a^b)^2 \sin(2\theta)}{s} \quad (16)$$

The following Eq. (17) defines the vantage point of an alpha capuchin when travelling normally and looking for nourishment on the ground:

$$k_a^b = k_a^b + C_a^b \quad (17)$$

The definition of Eq. (18), which describes how alpha the capuchins hang on trees in pursuit of nourishment, can be recast in the following manner:

$$k_a^b = C_a^b + L_{ab} \times \sin(\theta) \quad (18)$$

The location of alpha the capuchins while scaling trees to forage for food is described by the Eq.(19) that follows:

$$k_a^b = C_a^b + L_{ab}(U_a^b - U_{a-1}^b) \quad (19)$$

The definition of Eq.(20)'s depiction of the alpha capuchins' haphazard movement in seeking sources of food can be restated as follows:

$$k_a^b = \tau(\beta + (\chi - \beta)\delta()) \quad (20)$$

In the wild, capuchin monkeys forage efficiently by running, jumping, climbing and swinging, taking into account food availability, energy expenditure and environmental conditions. CapSA mimics these behaviors to develop an optimization algorithm for solving complex problems in different domains.

4. Results and Discussions

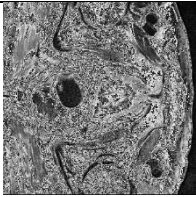
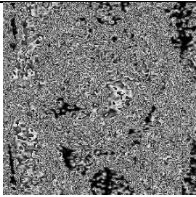
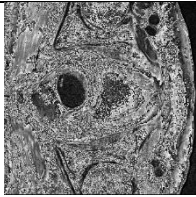
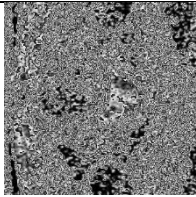
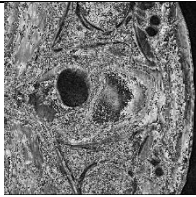
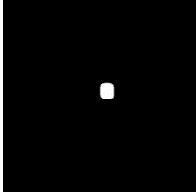
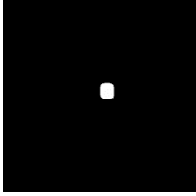
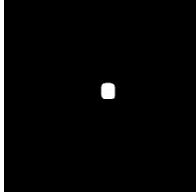


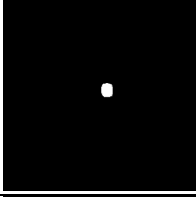
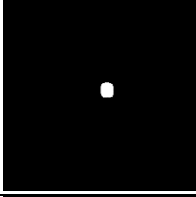
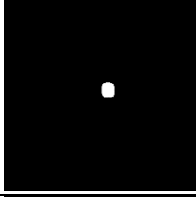
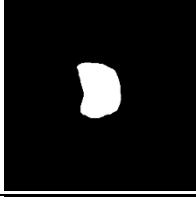
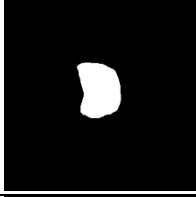
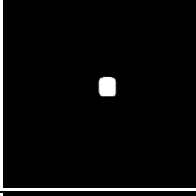
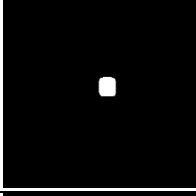
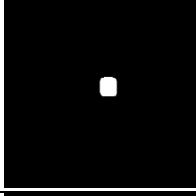
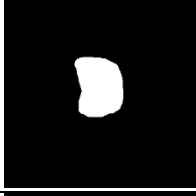
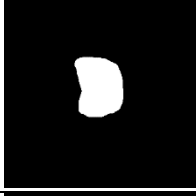
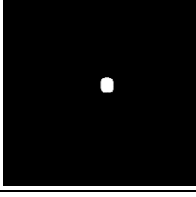
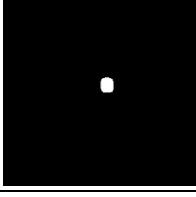
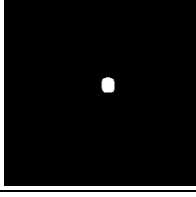
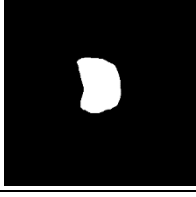
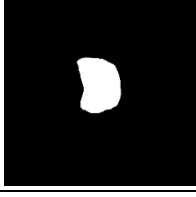
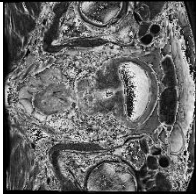
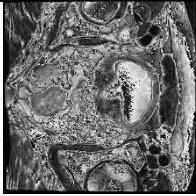
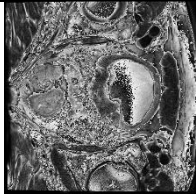
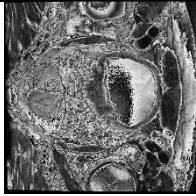
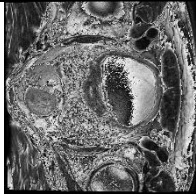
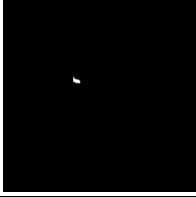
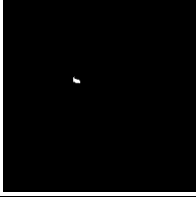
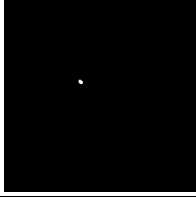
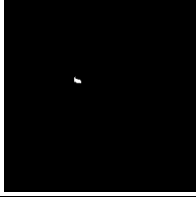
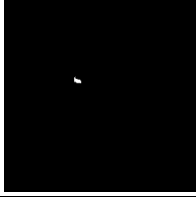
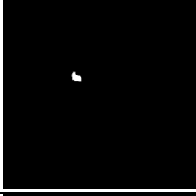
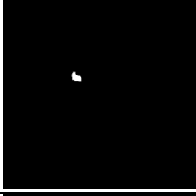
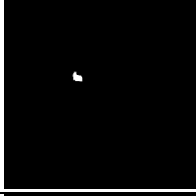
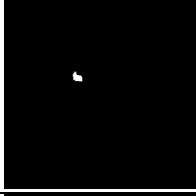
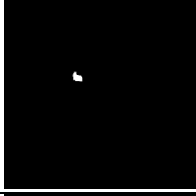
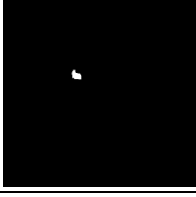
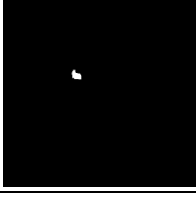
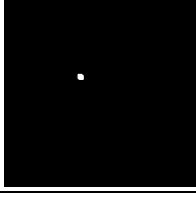
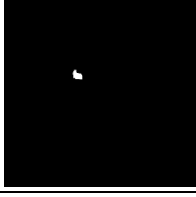
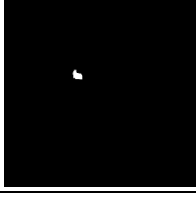
4.1. Experimental setup

The Python-based implementation of Evolutionary CapSA (ECapSA) for prostate cancer classification was carefully executed, followed by a series of comprehensive experiments. The developed model was trained for 50 iterations with a population size of 10 individuals. In this particular configuration, the chromosome length was set to 3 to ensure an optimal balance between complexity and computational efficiency.

Several advanced optimization methods were compared. These included traditional optimization methods such as Mine Blast Optimization (MBO)-AAMDNet [28], which simulates the blasting process to efficiently explore the search space; Chameleon Swarm Optimization (CSO)-AAMDNet [29], inspired by the adaptive and dynamic behaviour of chameleons; Archimedes Optimization Algorithm (AOA)-AAMDNet [30], which is based on Archimedes' principle to optimize solution search; and CapSA-AAMDNet a tailored optimization approach to improve classification accuracy.

4.2. Resultant images

The EcapSA-based prostate cancer classification system model has been executed, and it has generated a set of resulting images, which are presented in Fig. 7.

Description	Resultant images				
Images	1	2	3	4	5
	Dataset 1				
Original					
Ground Truth					
TransUnet Based Segmentation [32]					
Segnet Based Segmentation [33]					
DHS based segmented image					
	Dataset 2				
Original					
Ground Truth					
TransUnet based segmentation [32]					
Segnet based segmentation [33]					

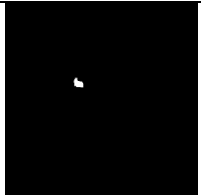
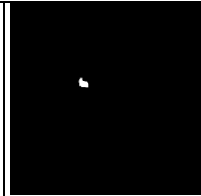
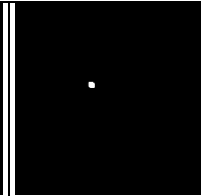
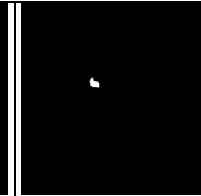
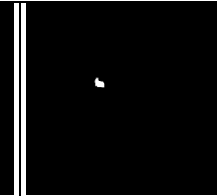
Description	Resultant images				
Images	1	2	3	4	5
	Dataset 1				
DHS based segmented image					

Fig. 7. Resultant images of two datasets for the enhanced CapSA based prostate cancer classification system model

4.3. Analysis of cost functions for two datasets using different algorithms

The proposed model was analyzed in detail using two different data sets, with a cost measure serving as the primary evaluation metric. The results of this analysis are shown in Fig. 8. A cost function was used to evaluate the profitability and efficiency of the developed model. This cost function was developed to estimate the overall profitability of the model considering various operational and computational costs.

In the experiments conducted, the cost measure was compared with different model designs over a range of iteration numbers from 0 to 50. In addition, the cost function was adjusted in a range from 2.5 to 6.0 to evaluate the performance of the model under different economic conditions. The graphical representation of these results can be seen in Fig. 8 and 9, which illustrate the cost-effectiveness of the model.

An important observation in Fig. 9 is the significant decrease in the cost function of the developed model when the iteration value is set to 10. This shows that the model quickly reaches an optimal state with minimal iterations.

The model shows a 72% reduction in the cost function compared to Mine Blast Optimization (MBO)-AAMDNet. This significant reduction underscores the model's ability to minimize costs while maintaining or improving performance. Compared to Chameleon Swarm Optimization (CSO)-AAMDNet, the proposed model shows a 63% reduction in the cost function. This comparison underlines the economic advantage of the new model over conventional optimization methods.

Compared to Archimedes Optimization Algorithm (AOA)-AAMDNet, the developed model achieves a cost reduction of 74. The cost function of the proposed model is 75% lower than that of CapSA-AAMDNet. This reduction indicates a significant improvement in economic efficiency and positions the new model as a cost-effective alternative. The results clearly show that the recommended model has a significantly lower cost function compared to the other models.

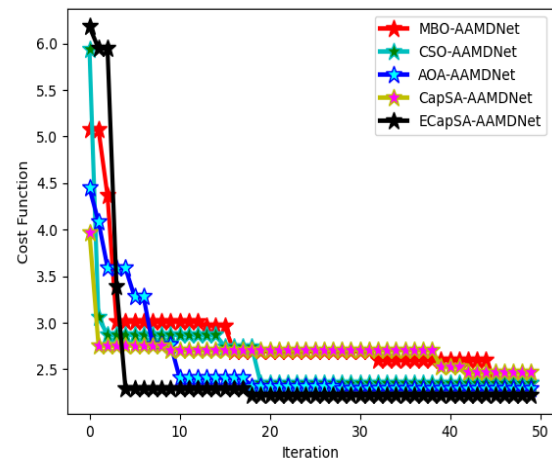


Fig. 8. Cost function analysis of the suggested ECapSA based prostate cancer classification system model regarding Dataset 1

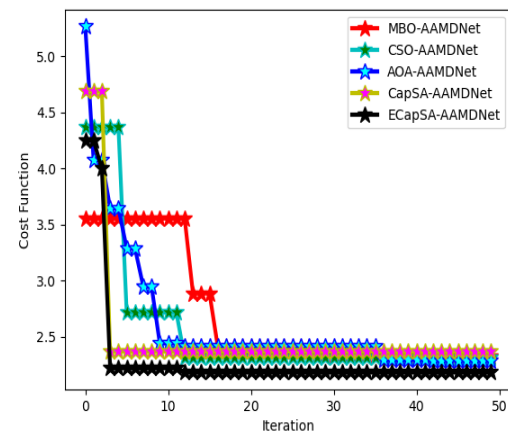


Fig. 9. Cost function analysis of the suggested ECapSA based prostate cancer classification system model regarding Dataset 2

4.4. ROC analysis of the two datasets for the developed model over various classifiers

The ROC curve (Receiver Operating Characteristic) is an important tool for evaluating the accuracy of a system. Figure 10 shows the analysis of the ROC curve of the proposed model applied to two datasets and compared with existing classifiers. In this analysis, the performance of the model is evaluated by varying the rate of true-positive (TPR) and false-positive (FPR) results from 0 to 1.

Figure 10 shows that the proposed model performs significantly better than conventional models at a false positive rate of 0.2.

Specifically, it shows a 29% improvement over ResNet, a 30% improvement over Inception, a 31% improvement over MobileNet, and an impressive 31.5% improvement over AAMDNet. These results emphasise the improved efficiency and effectiveness of the recommended model.

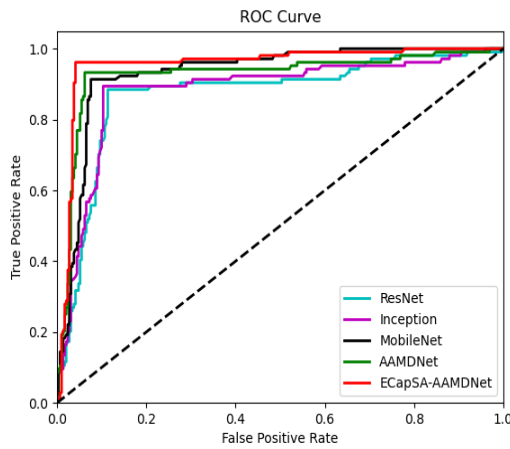


Fig. 10. Cost function analysis of the suggested ECapSA based prostate cancer classification system model regarding Dataset 1

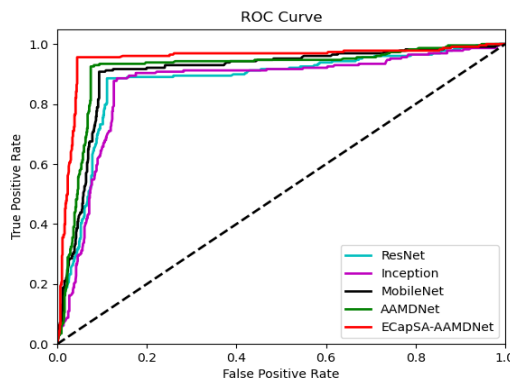


Fig. 11. Cost function analysis of the suggested ECapSA based prostate cancer classification system model regarding Dataset 2

4.5. Segmentation analysis of the developed model for two datasets over distinct classifiers

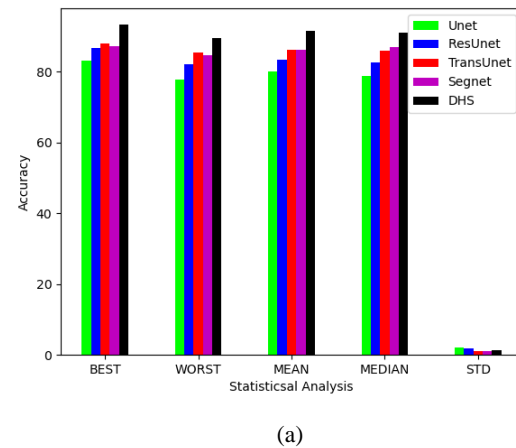
The segmentation performance of the proposed system for two datasets is evaluated in detail in Figures 10 and 11. These figures provide a comprehensive statistical comparison between the proposed model and several existing classifiers. The evaluation includes various statistical measures such as the best, worst, mean, standard deviation and median for accuracy, Dice coefficient and Jaccard index.

Figure 12 focuses on the best performance measures and shows that the proposed system has significant improvements over other models. Looking at the best accuracy measure, the recommended system shows remarkable progress:

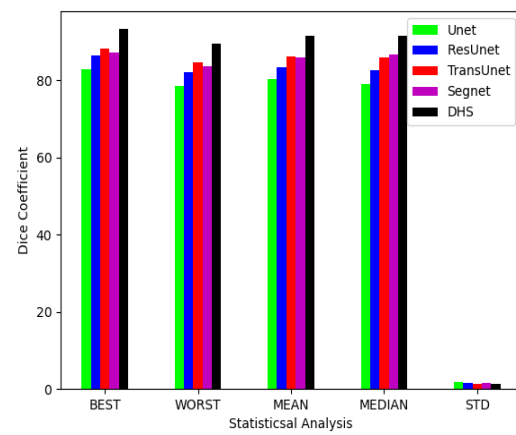
- An 87% increase in accuracy compared to Unet.
- An 85% increase compared to Resunet.
- A 97% increase compared to TransUnet.
- An impressive 98% increase compared to Segnet.

These significant improvements underline the superior efficiency and effectiveness of the developed model. The comparison shows that the proposed system excels not only in accuracy, but also in other critical segmentation performance metrics. This comprehensive analysis confirms the advanced capabilities of the

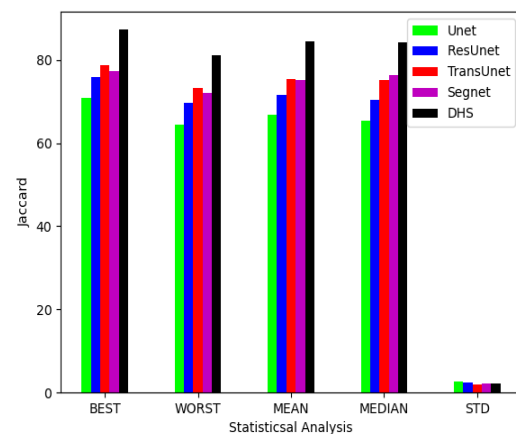
proposed model and shows that it has the potential to outperform traditional segmentation methods in various datasets and performance metrics.



(a)

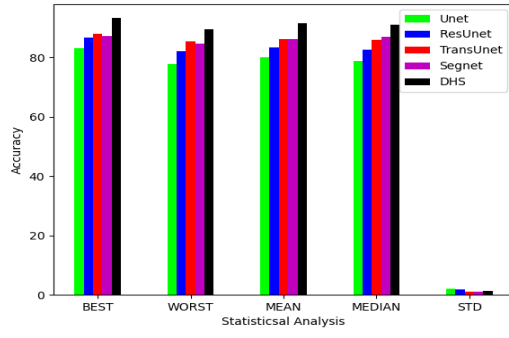


(b)

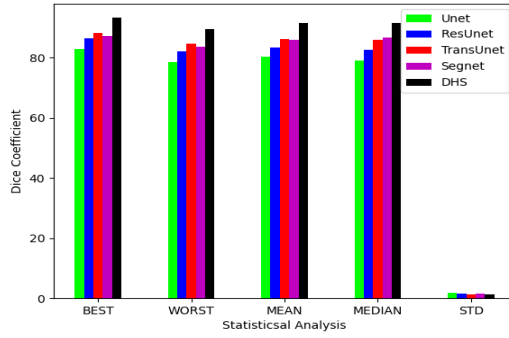


(c)

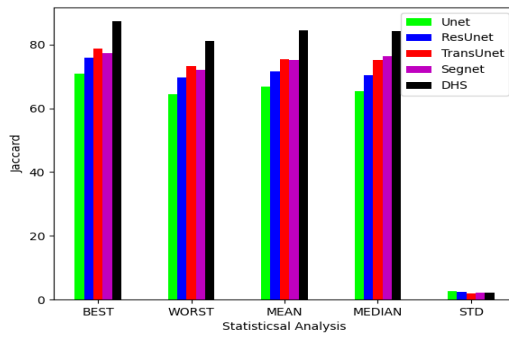
Fig. 12. Statistical analysis for suggested ECapSA based prostate cancer segmentation system model regarding contrasted with distinct traditional classifier in dataset 1 concerning “(a) Accuracy, (b) Dice coefficient, (c) Jaccard”



(a)



(b)



(c)

Fig. 13. Statistical analysis for suggested ECapSA based prostate cancer segmentation system model regarding contrasted with distinct traditional classifier in dataset 2 concerning “(a) Accuracy, (b) Dice coefficient, (c) Jaccard”

4.6. K-fold of performance of two datasets for the developed model over distinct algorithms and classifiers

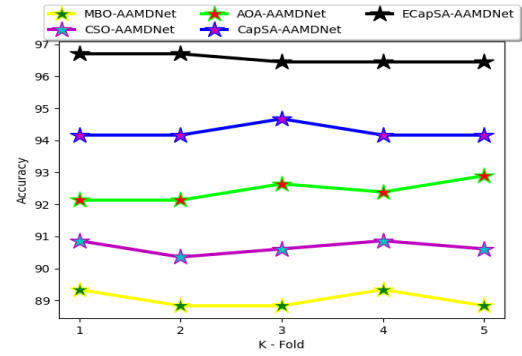
The K-fold evaluation of the recommended system for different models and classifiers is shown in Figures 12 and 13. These figures illustrate the K-fold evaluation of the proposed model using the original dataset compared to different algorithms and classifiers. In addition, Figures 14 and 15 show the K-fold evaluation of the recommended model using the second dataset compared to different optimization models and classifiers.

The K-fold measure, which ranges from 1 to 5, is used to evaluate the performance of the model when applied to new data. Figure 14(a) shows that the recommended model shows a significant improvement in accuracy at a K-fold measure of 3, and in particular achieves the following values:

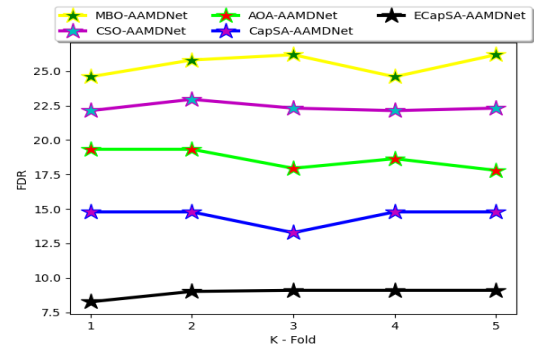
- A 26% increase over MBO-AAMDNet
- A 28% increase compared to CSO-AAMDNet

- A 28.6% increase compared to AOA-AAMDNet
- A 30% increase compared to CapSA-AAMDNet

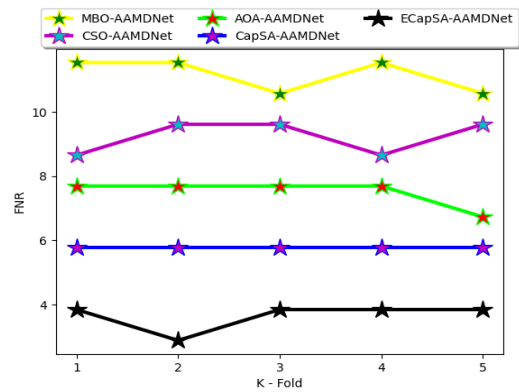
These significant improvements underline the robustness and effectiveness of the recommended model when confronted with new data.



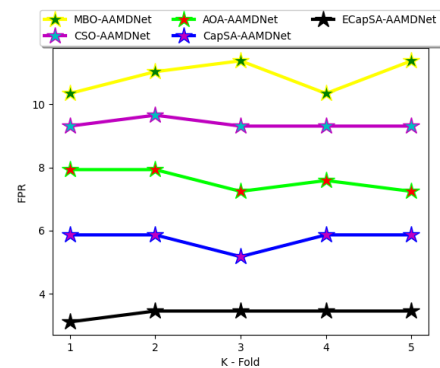
(a)



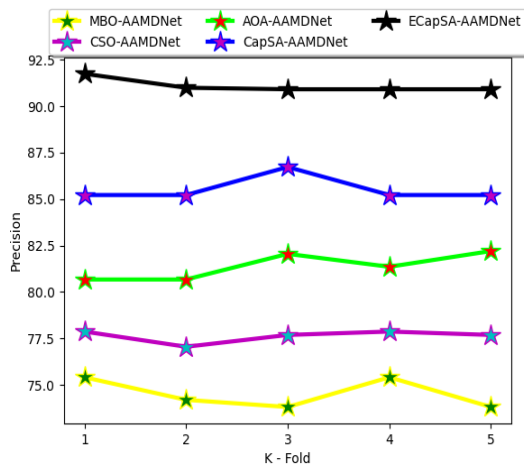
(b)



(c)

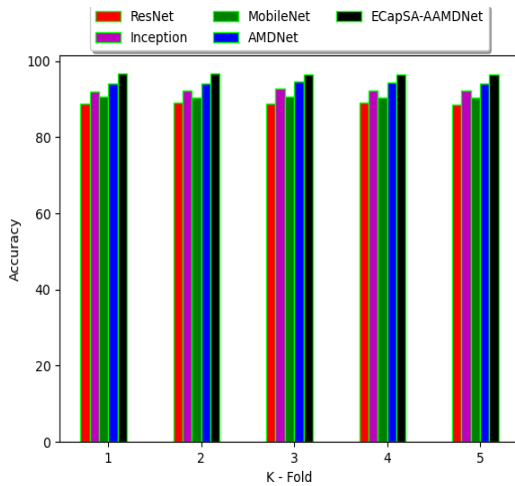


(d)

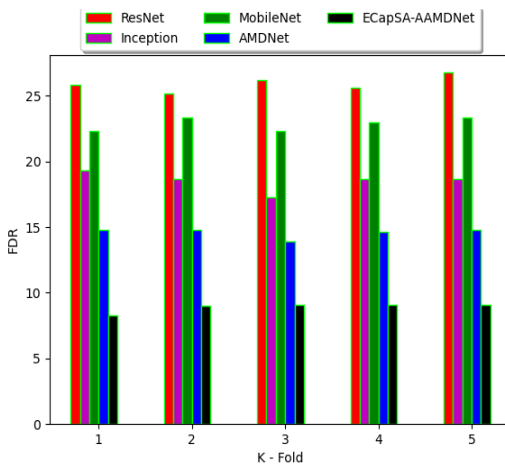


(e)

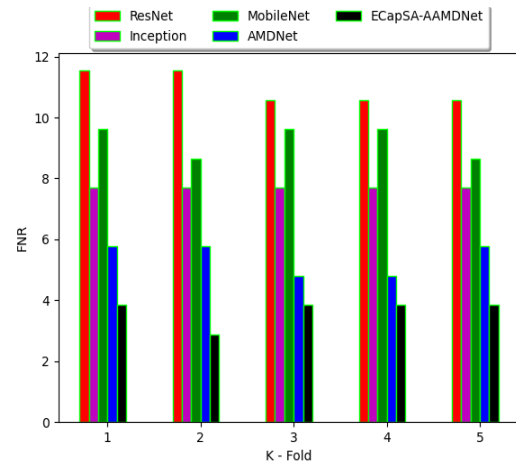
Fig. 14. K-fold analysis of the recommended ECapSA based prostate cancer classification system model contrasted with distinct traditional algorithm in dataset 1 concerning “(a) Accuracy, (b) FDR, (c) FNR, (d) FPR and (e) Precision”



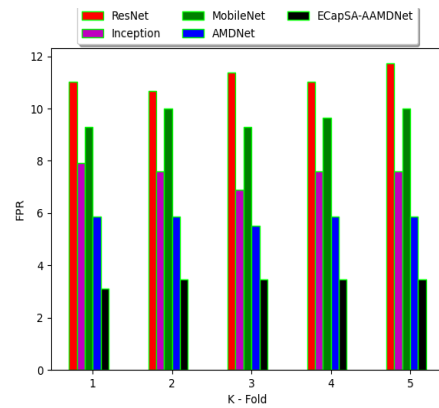
(a)



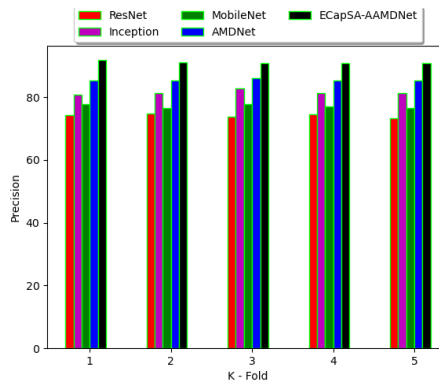
(b)



(c)

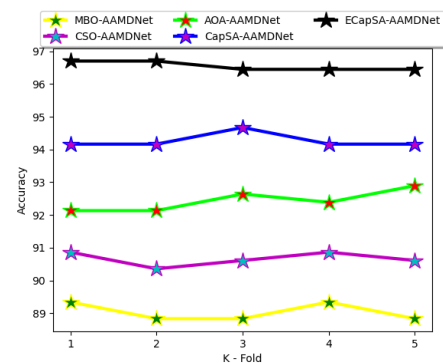


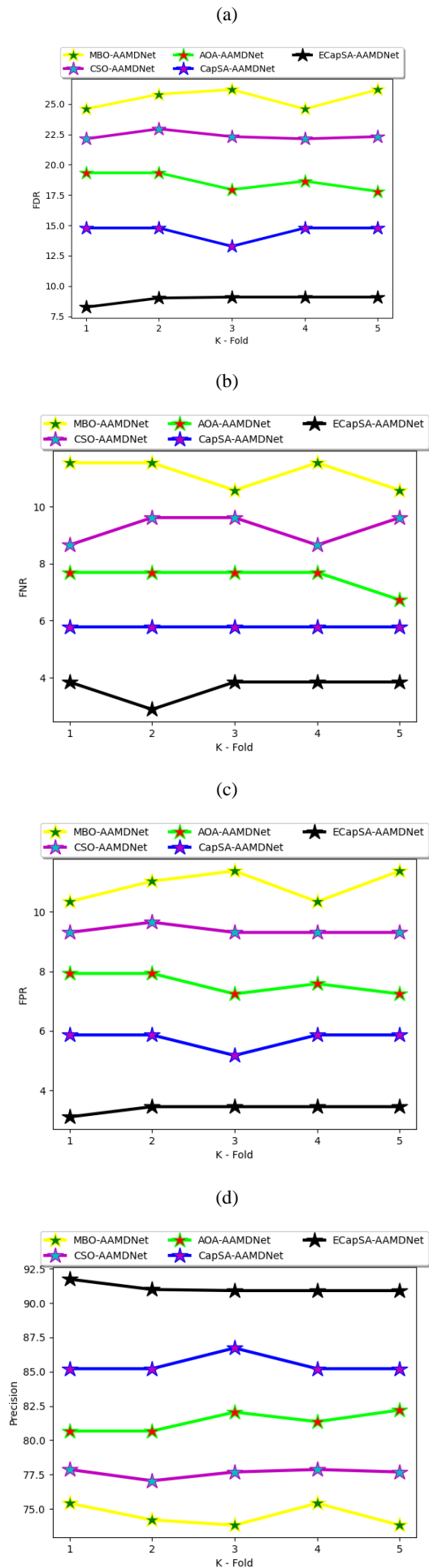
(d)



(e)

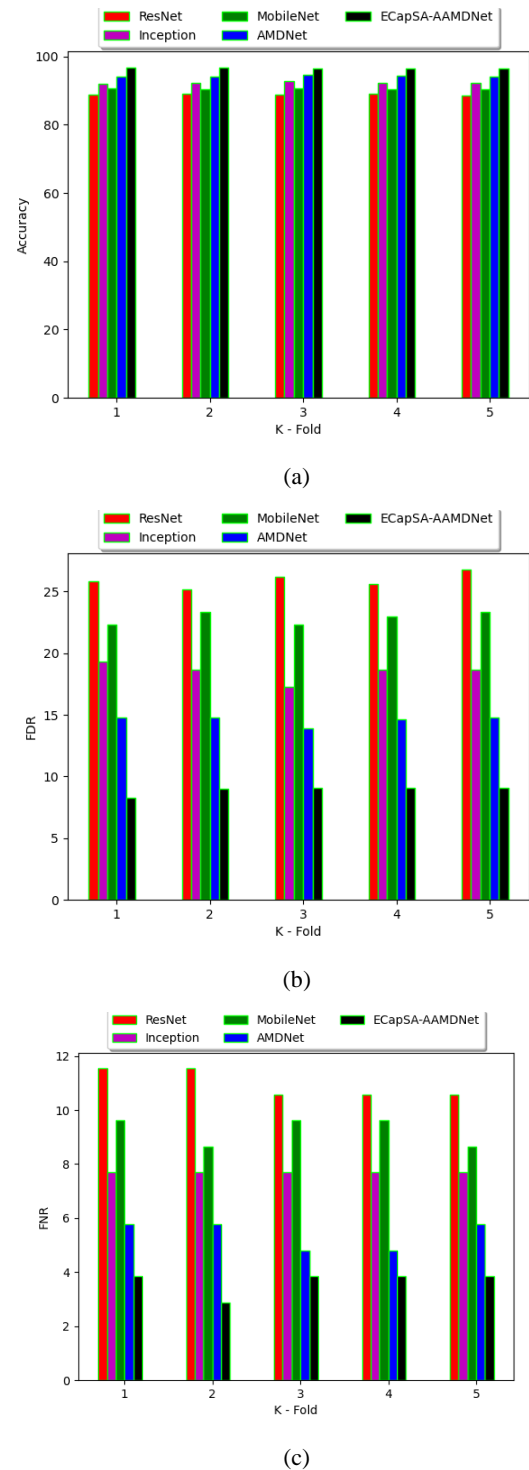
Fig. 15. K-fold analysis of the recommended ECapSA based prostate cancer classification system model contrasted with distinct traditional classifier in dataset 1 concerning “(a) Accuracy, (b) FDR, (c) FNR, (d) FPR and (e) Precision”

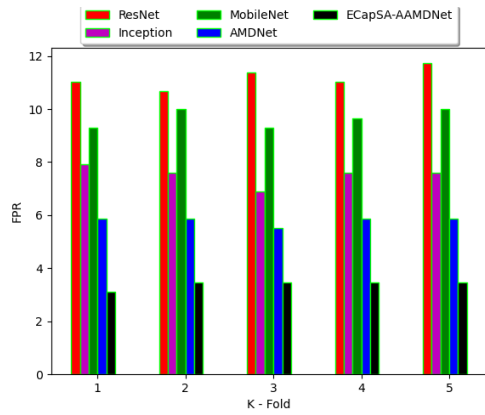




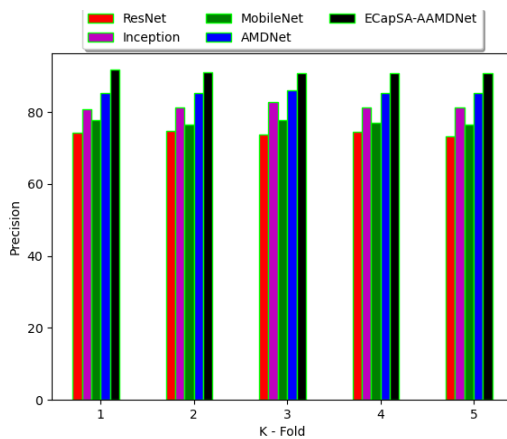
(e)

Fig. 16. K-fold analysis of the recommended ECapSA based prostate cancer classification system model contrasted with distinct traditional algorithm in dataset 2 concerning “(a) Accuracy, (b) FDR, (c) FNR, (d) FPR and (e) Precision





(d)



(e)

Fig. 17. K-fold analysis of the recommended ECapSA based prostate cancer classification system model contrasted with distinct traditional classifier in dataset 2 concerning “(a) Accuracy, (b) FDR, (c) FNR, (d) FPR and (e) Precision”

4.7. K-fold comparative analysis of two datasets for the developed model over distinct algorithms and classifiers

The K-fold performance evaluation of the developed model on two datasets with conventional algorithms and classifiers is summarized in Table II and Table III, respectively. These tables provide a detailed comparison of the performance of the model with different conventional algorithms and classifiers, which illustrates the effectiveness of the developed model.

In particular, the evaluation of the second dataset shows remarkable performance, with the recommended model achieving an accuracy of 99.49%. This outstanding performance far outperforms other conventional models and highlights several important points:

4.7.1. Accuracy

The accuracy of 99.49% in the second data set shows that the developed model correctly identifies and segments the data with an exceptionally high precision. This is a clear indication of the model's advanced ability to process complex data sets and deliver reliable results.

4.7.2. Comparison with conventional models

The performance of the recommended model is significantly better compared to conventional models. The accuracy metrics of conventional models fall in comparison, highlighting the advanced

algorithms and optimization techniques of the developed model that contribute to its higher performance.

4.7.3. Robustness and reliability

The high accuracy rate in the second data set in Table III confirms the robustness and reliability of the recommended model. It proves the ability of the model to perform consistently well even with different and potentially difficult datasets.

4.7.4. Comprehensive evaluation

The K-fold performance evaluation methodology provides a comprehensive assessment of the model's capabilities. Splitting the data into multiple subsets and assessing the model's performance across these subsets ensures that the model's high performance is not due to over fitting, but reflects the model's efficiency. In summary, the K-fold performance evaluation summarized in Table II and Table III clearly demonstrates the superior performance of the developed model. Its impressive accuracy of 99.49% on the second data set is a testament to its advanced design and effectiveness, setting a new benchmark for segmentation models in this field.

Table II: K-Fold Comparative Analysis of the Developed Ecapsa Based Prostate Cancer Classification System Model Over Distinct Algorithms for Two Datasets

TERMS	MBO-AAMD Net [27]	CSOAAMD Net [28]	AOA-AAMD Net [29]	CapSA-AAMD Net [26]	Proposed ECapSA-AAMDNet
Accuracy	88.83	90.60	92.89	94.16	96.44
Sensitivity	89.42	90.38	93.26	94.23	96.15
Specificity	88.62	90.68	92.75	94.13	96.55
Precision	73.80	77.68	82.20	85.21	90.90
FPR	11.37	9.31	7.24	5.86	3.44
FNR	10.57	9.61	6.73	5.76	3.84
NPV	95.89	96.33	97.46	97.84	98.59
FDR	26.19	22.31	17.79	14.78	9.09
F1-Score	80.86	83.55	87.38	89.49	93.45
MCC	0.73	0.77	0.82	0.85	0.91
Dataset-2					
Accuracy	89.56	88.18	92.05	93.53	96.30
Sensitivity	89.91	89.47	92.54	93.42	96.05
Specificity	89.47	87.83	91.92	93.56	96.37
Precision	69.49	66.23	75.35	79.47	87.60
FPR	10.52	12.16	8.07	6.43	3.62
FNR	10.08	10.52	7.45	6.57	3.94
NPV	97.08	96.90	97.88	98.15	98.91
FDR	30.50	33.76	24.64	20.52	12.40
F1-Score	78.39	76.11	83.07	85.88	91.63
MCC	0.72	0.69	0.78	0.82	0.89

Table III: K-Fold Comparative Analysis of the Developed Ecapsa Based Prostate Cancer Classification System Model Over Distinct Classifiers for Two Datasets

TERMS	Resnet [34]	Inception [35]	Mobile Net [36]	AMD Net	Proposed ECapSA-AAMDNet
Dataset-1					
Accuracy	88.57	92.38	90.35	94.16	96.44
Sensitivity	89.42	92.30	91.34	94.23	96.15
Specificity	88.27	92.41	90	94.13	96.55
Precision	73.22	81.35	76.61	85.21	90.90
FPR	11.72	7.58	10	5.86	3.44
FNR	10.57	7.69	8.65	5.76	3.84
NPV	95.88	97.10	96.66	97.84	98.59
FDR	26.77	18.64	23.38	14.78	9.09

F1-Score	80.51	86.48	83.33	89.49	93.45
MCC	0.73	0.81	0.77	0.85	0.91
Dataset-2					
Accuracy	90.76	88.73	92.42	94.36	96.30
Sensitivity	90.78	88.59	92.54	94.29	96.05
Specificity	90.76	88.77	92.39	94.38	96.37
Precision	72.37	67.78	76.44	81.74	87.6
FPR	9.23	11.22	7.60	5.61	3.62
FNR	9.21	11.40	7.45	5.70	3.94
NPV	97.36	96.68	97.89	98.41	98.91
FDR	27.62	32.21	23.55	18.25	12.4
F1-Score	80.54	76.80	83.73	87.57	91.63
MCC	0.75	0.70	0.79	0.84	0.89

5. Conclusion

An ECapSA-based classification system for prostate cancer was developed that uses hybrid deep learning models to identify diseases. First, input images were collected from public online sources to obtain a diverse and representative dataset. A combination of advanced computer vision techniques, in particular TransUnet and SegNet, was applied to accurately segment the prostate regions in the input images. Effective segmentation was critical for isolating areas of interest and improving subsequent classification. The AAMDNet was implemented as a classification model, using the segmented images as input to the AAMDNet, which categorized them into cancerous and non-cancerous categories. The goal was to achieve high classification accuracy by utilizing the power of deep learning. Finally, the performance of the proposed approach was validated using various evaluation metrics. The metrics used to evaluate the effectiveness of the model included sensitivity, specificity, F1 score, accuracy.

A thorough evaluation ensured that the model was reliable and accurate in classifying prostate cancer. The effectiveness of deep learning models such as AAMDNet depends heavily on the quantity and quality of the training data. When looking at the accuracy measure, it is clear that the recommended system shows significant improvements over other models. In particular, it achieves a 57% increase in accuracy compared to Unet, a 55% increase compared to Resunet, a 67% increase compared to TransUnet and an impressive 48% increase compared to Segnet. This confirms that the developed model has a higher efficiency compared to the other models. If the data set used was small or not representative of the population, this could lead to biased or inaccurate results. Addressing the limitations and exploring these future areas can contribute to the continuous improvement and effectiveness of the proposed prostate cancer classification system. It is important to work closely together with healthcare professionals and follow ethical guidelines throughout the development and deployment process.

References

- [1]. J. Broomfield, "Handheld ISFET Lab-on-Chip Detection of TMPRSS2-ERG and AR mRNA for Prostate Cancer Prognostics," *IEEE Sensors Letters*, vol. 7, no. 8, pp. 1-4, Aug. 2023, Art no. 4501504.
- [2]. Y. Qian, Z. Zhang and B. Wang, "ProCDet: A New Method for Prostate Cancer Detection Based on MR Images," *IEEE Access*, vol. 9, pp. 143495-143505, 2021.
- [3]. G. Li and H. Li, "Linear Model Selection and Regularization for Serum Prostate-Specific Antigen Prediction of Patients With Prostate Cancer Using R," *IEEE Access*, vol. 9, pp. 97591-97602, 2021.
- [4]. L. Gorelick et al., "Prostate Histopathology: Learning Tissue Component Histograms for Cancer Detection and Classification," *IEEE Transactions on Medical Imaging*, vol. 32, no. 10, pp. 1804-1818, Oct. 2013.
- [5]. A. G. Chung, F. Khalvati, M. J. Shafiee, M. A. Haider and A. Wong, "Prostate Cancer Detection via a Quantitative Radiomics-Driven Conditional Random Field Framework," *IEEE Access*, vol. 3, pp. 2531-2541, 2015.
- [6]. C. Mosquera-Lopez, S. Agaian, A. Velez-Hoyos and I. Thompson, "Computer-Aided Prostate Cancer Diagnosis From Digitized Histopathology: A Review on Texture-Based Systems," *IEEE Reviews in Biomedical Engineering*, vol. 8, pp. 98-113, 2015.
- [7]. Y. Feng, "A Deep Learning Approach for Targeted Contrast-Enhanced Ultrasound Based Prostate Cancer Detection," *IEEE/ACM Transactions on Computational Biology and Bioinformatics*, vol. 16, no. 6, pp. 1794-1801, 1 Nov.-Dec. 2019.
- [8]. H. Aoyama, Y. Azuma and K. Inamura, "Comparison of Daily Prostate Positions during Conformal Radiation Therapy of Prostate Cancer Using an Integrated CT-linear Accelerator System: In-room CT Image versus Digitally Reconstructed Radiograph," *Journal of Radiation Research*, vol. 52, no. 2, pp. 220-228, March 2011.
- [9]. Y. -Y. Zhang, Q. Li, Y. Xin and W. -Q. Lv, "Differentiating Prostate Cancer from Benign Prostatic Hyperplasia Using PSAD Based on Machine Learning: Single-Center Retrospective Study in China," *IEEE/ACM Transactions on Computational Biology and Bioinformatics*, vol. 16, no. 3, pp. 936-941, 1 May-June 2019.
- [10]. G. Litjens, O. Debats, J. Barentsz, N. Karssemeijer and H. Huisman, "Computer-Aided Detection of Prostate Cancer in MRI," *IEEE Transactions on Medical Imaging*, vol. 33, no. 5, pp. 1083-1092, May 2014.
- [11]. Shekoofeh Azizi; Sharareh Bayat; Pingkun Yan; Amir Tahmasebi; Jin Tae Kwak; Sheng X, "Deep Recurrent Neural Networks for Prostate Cancer Detection: Analysis of Temporal Enhanced Ultrasound," *IEEE Transactions on Medical Imaging*, vol. 37, no. 12, pp. 2695-2703, Dec. 2018.
- [12]. Y. Artan and I. S. Yetik, "Prostate Cancer Localization Using Multiparametric MRI based on Semisupervised Techniques With Automated Seed Initialization," *IEEE Transactions on Information Technology in Biomedicine*, vol. 16, no. 6, pp. 1313-1323, Nov. 2012.
- [13]. J. T. Kwak and S. M. Hewitt, "Nuclear Architecture Analysis of Prostate Cancer via Convolutional Neural Networks," *IEEE Access*, vol. 5, pp. 18526-18533, 2017.
- [14]. Wenyuan Li; Jiayun Li; Karthik V. Sarma; King Chung Ho; Shiwen Shen; Beatrice S. Knudse, "Path R-CNN for Prostate Cancer Diagnosis and Gleason Grading of Histological Images," *IEEE Transactions on Medical Imaging*, vol. 38, no. 4, pp. 945-954, April 2019.
- [15]. Youngho Seo, J. Kurhanewicz, B. L. Franc, R. A. Hawkins and B. H. Hasegawa, "Improved prostate cancer imaging with SPECT/CT and MRI/MRSI," *IEEE Transactions on Nuclear Science*, vol. 52, no. 5, pp. 1316-1320, Oct. 2005.
- [16]. Shrestha, S., Alsadoon, A., Prasad, P.W.C. "A novel solution of using deep learning for prostate cancer segmentation: enhanced batch normalization". *Multimedia Tools Application* Vol.80, 21293-21313, 2021.
- [17]. Garg, G., Juneja, M. "Particle swarm optimization based segmentation of Cancer in multi-parametric prostate MRI". *Multimed Tools Application* Vol.80, 30557-30580, 2021.

- [18]. Chahal, E.S., Patel, A., Gupta. "Unet based Xception Model for Prostate Cancer Segmentation from MRI Images". *Multimed Tools Application* Vol.81, 37333–37349, 2022.
- [19]. Guiqin Liu, Shihang Pan, Rui Zhao, Huang Zhou, Jie Chen, Xiang Zhou, Jianrong Xu, Yan Zhou, Wei Xue and Guangyu Wu. "The added value of AI-based computer-aided diagnosis in classification of cancer at prostate MRI". *European Radiology* Vol.33, 5118–5130, 2023.
- [20]. Pääkkönen, J., Päivinen, N., Nykänen. "An automated gland segmentation and classification method in prostate biopsies: an image source-independent approach". *Machine Vision and Applications* 26, 103–113, 2015.
- [21]. Pushpak Pati , Guillaume Jaume , Zeineb Ayadi , Kevin Thandiackal , Behzad Bozorgtabar , Maria Gabrani , Orcun Goksel "Weakly supervised joint whole-slide segmentation and classification in prostate cancer" *Medical Image Analysis* Volume 89, 102915, October 2023.
- [22]. Yuchun Li; Mengxing Huang; Yu Zhang; Jing Chen; Haixia Xu; Gang Wang; Wenlong Feng, "Automated Gleason Grading and Gleason Pattern Region Segmentation Based on Deep Learning for Pathological Images of Prostate Cancer," *IEEE Access*, vol. 8, pp. 117714-117725, 2020
- [23]. Cancer center AI <<https://cancer-center.ai/database>> National Cancer Institute 2023-09-26
- [24]. R. Pei et al., "Real-Time Multi-Focus Biomedical Microscopic Image Fusion Based on m-SegNet," *IEEE Photonics Journal*, vol. 13, no. 3, pp. 1-18, June 2021, Art no. 8600118.
- [25]. A. Krueangsai and S. Supratid, "Effects of Shortcut-Level Amount in Lightweight ResNet of ResNet on Object Recognition with Distinct Number of Categories," 2022 International Electrical Engineering Congress (iEECON), Khon Kaen, Thailand, 2022, pp. 1-4.
- [26]. X. Zhao, H. Zhang, Y. Zhang, T. K. Sarkar and S. -W. Ting, "Efficient Modeling of Multiscale Structures Using Higher-Order Method of Moments," *IEEE Journal on Multiscale and Multiphysics Computational Techniques*, vol. 2, pp. 78-83, 2017.
- [27]. X. Ding et al., "Distribution Characteristics of Fragments Size and Optimization of Blasting Parameters Under Blasting Impact Load in Open-Pit Mine," *IEEE Access*, vol. 7, pp. 137501-137516, 2019.
- [28]. A. Uluslu, "Chameleon Swarm Algorithm Assisted Optimization of U-Slot Patch Antenna for Quad-Band Applications," *IEEE Access*, vol. 10, pp. 74152-74163, 2022.
- [29]. T. -T. Nguyen, T. -K. Dao, T. -T. -T. Nguyen and T. -D. Nguyen, "An Optimal Microgrid Operations Planning Using Improved Archimedes Optimization Algorithm," *IEEE Access*, vol. 10, pp. 67940-67957, 2022.
- [30]. J. S. Suri et al., "UNet Deep Learning Architecture for Segmentation of Vascular and Non-Vascular Images: A Microscopic Look at UNet Components Buffered With Pruning, Explainable Artificial Intelligence, and Bias," in *IEEE Access*, vol. 11, pp. 595-645, 2023.
- [31]. V. Donthula, B. Camps-Raga, N. E. Islam, A. Slusarz, D. B. Lubahn and V. Ganjam, "Effects of nanosecond pulsed electric fields on the human prostate cancer cell line LNCaP," *IEEE Transactions on Dielectrics and Electrical Insulation*, vol. 16, no. 5, pp. 1311-1316, October 2009.
- [32]. H. Xu, S. Park and T. H. Hwang, "Computerized Classification of Prostate Cancer Gleason Scores from Whole Slide Images," *IEEE/ACM Transactions on Computational Biology and Bioinformatics*, vol. 17, no. 6, pp. 1871-1882, 1 Nov.-Dec. 2020.
- [33]. Z. Xu et al., "Inversion of the Gravity Gradiometry Data by ResUnet Network: An Application in Nordkapp Basin, Barents Sea," *IEEE Transactions on Geoscience and Remote Sensing*, vol. 61, pp. 1-10, 2023, Art no. 4502410.
- [34]. Y. Yang and S. Mehrkanoon, "AA-TransUNet: Attention Augmented TransUNet For Nowcasting Tasks," 2022 International Joint Conference on Neural Networks (IJCNN), Padua, Italy, 2022, pp. 01-08.
- [35]. G. V. Naidis, "Discharge Inception in Hydrocarbon Liquids: Effect of Electrode Surface Roughness," *IEEE Transactions on Dielectrics and Electrical Insulation*, vol. 29, no. 1, pp. 347-349, Feb. 2022.
- [36]. H. Pan, Z. Pang, Y. Wang, Y. Wang and L. Chen, "A New Image Recognition and Classification Method Combining Transfer Learning Algorithm and MobileNet Model for Welding Defects," *IEEE Access*, vol. 8, pp. 119951-119960, 2020.